Journal of ELECTRONIC MATERIALS, Vol. 45, No. 3, 2016
DOI: 10.1007/s11664-015-4050-8
© 2015 The Minerals, Metals & Materials Society

Development of Thermoelectric Fibers for Miniature Thermoelectric Devices

FEI REN,[1,3] PAUL MENCHHOFER,[2] JAMES KIGGANS,[2] and HSIN WANG[2,4]

1.—Mechanical Engineering, Temple University, Philadelphia, PA 19122, USA. 2.—Materials Science and Technology Division, Oak Ridge National Laboratory, Oak Ridge, TN 37830, USA. 3.—e-mail: renfei@temple.edu. 4.—e-mail: wangh2@ornl.gov

Miniature thermoelectric (TE) devices may be used in a variety of applications such as power sources of small sensors, temperature regulation of precision electronics, etc. Reducing the size of TE elements may also enable design of novel devices with unique form factor and higher device efficiency. Current industrial practice of fabricating TE devices usually involves mechanical removal processes that not only lead to material loss but also limit the geometry of the TE elements. In this project, we explored a powder-processing method for the fabrication of TE fibers with large length-to-area ratio, which could be potentially used for miniature TE devices. Powders were milled from Bi_2Te_3-based bulk materials and then mixed with a thermoplastic resin dissolved in an organic solvent. Through an extrusion process, flexible, continuous fibers with sub-millimeter diameters were formed. The polymer phase was then removed by sintering. Sintered fibers exhibited similar Seebeck coefficients to the bulk materials. However, their electrical resistivity was much higher, which might be related to the residual porosity and grain boundary contamination. Prototype miniature uni-couples fabricated from these fibers showed a linear *I–V* behavior and could generate millivolt voltages and output power in the nano-watt range. Further development of these TE fibers requires improvement in their electrical conductivities, which needs a better understanding of the causes that lead to the low conductivity in the sintered fibers.

Key words: Thermoelectrics, powder processing, fiber, power generator, composite

INTRODUCTION

Development of high-performance thermoelectric (TE) devices requires improvements in material transport properties, reflected by the figure of merit, *ZT*, which determines the material's performance and device efficiency. Meanwhile, enhancement can also be achieved through advancement in device design. For example, by stacking the *n*-type and *p*-type TE elements in the heat flow direction, one may shorten the electrical current path through shunts and thus reduce parasitic losses.[1] TE elements with unique form factors may play an important role in enabling novel applications. For applications involving low power and small temperature gradient, such as body heat harvesters and power sources of wireless sensors, miniature TE elements with large length-to-area ratio are preferred in order to meet the requirements of output power and voltage.[2]

Most commercial TE devices are constructed from individual elements that are connected by metallic contacts.[3,4] These individual elements are typically fabricated using a series of mechanical removal processes including cutting, grinding, and polishing. Joining techniques such as soldering or diffusion bonding are usually used to package TE elements with metal contacts and insulation materials. Generally, this machining approach not only encounters

(Received May 21, 2015; accepted September 8, 2015; published online September 23, 2015)

non-trivial material loss (c.a. 30–70%) but also limits the obtainable geometry of the TE elements. Recently, micromachining has been proposed to fabricate miniature TE generators,[5] which was soon demonstrated in practice in the fabrication of miniature devices with TE elements of large aspect ratios using high-precision machining and appropriate packaging technologies.[2,6]

On the other hand, additive manufacturing techniques, such as printing, have been explored in the fabrication of miniature TE devices. Printing has been traditionally used with organic and polymeric composite TE materials;[7,8] but in recent years it has gained popularity in the processing of inorganic TE materials. For example, thick films (up to 200 μm) were fabricated by printing pastes of Bi_2Te_3 and Sb_2Te_3 powders mixed with epoxies.[9] Using a similar approach, Kim et al. designed and fabricated a flexible TE generator that consisted of 12 uni-couples and generated up to 147 nW energy when attached to a human body.[10] Since substrates are usually used in such printing processes, the fabrication of freestanding TE elements is difficult. In addition, the existence of substrates (e.g., polyimides) may limit further treatment (e.g., annealing) of the TE elements.

In addition to printing, drawing has also been used in fabrication of TE elements. In a recent work by Shiota et al.,[11] molten Bi_2Te_3 was sealed in glass tubes and drawn through a 1-mm die. The resulting product was glass-encapsulated Bi_2Te_3 fibers that were ~75 μm in diameter. The resultant TE fibers were difficult to separate from the glass envelope. Furthermore, since this process is conducted at high temperatures, it demands special equipment and accurate process control.

Therefore, new manufacturing techniques, which are simple, cost effective, and capable of fabricating small TE elements with unconventional form factors (e.g., very large length-to-area ratio), will benefit from the research and development of miniature TE devices.

In this study, we explored the feasibility of a powder-processing-based method in the fabrication of TE fibers. This extrusion technique was originally utilized to create fibrous monolithic ceramics.[12] This approach, when modified and applied to our TE materials, was capable of fabricating freestanding, continuous fibers with diameters in the range of hundreds of microns. In the following sections, details of fiber fabrication will be explained, followed by discussion of the microstructure and electrical properties of the fibers, as well as their performance when used to construct prototype uni-couples. Potential strategies to further improve material properties will also be discussed.

MATERIALS AND METHODS

Materials used in this study were synthesized by reacting pure elements in fused silica ampoules. The nominal compositions were $Bi_{0.4}Sb_{1.6}Te_3$ for the *p*-type and $Bi_2Te_{2.7}Se_{0.3}$ for the *n*-type materials. Details of material synthesis can be found elsewhere.[13] Ingots were crushed and milled using a high-energy ball mill (8000M; SPEX SamplePrep, Metuchen, NJ, USA) for 10 min. Powders were sieved to −325 mesh. Milling and sieving were performed in inert atmosphere to prevent powders from oxidation.

Paraloid B-72 thermoplastic resin (Rohm and Haas, Philadelphia, PA, USA) was first dissolved in methyl ethyl ketone (MEK) at a 50 wt.% concentration. Milled TE powders were then added into the B-72/MEK solution and mechanically mixed to form a paste. The volumetric ratio between the TE powder and the B-72 (excluding the MEK) was 1:1. The paste was then loaded into syringes and manually extruded to form fibers. The MEK solvent was allowed to evaporate during overnight drying in air at room temperature, resulting in TE/B-72 composite fibers. The composite fibers were sintered either under vacuum or flowing Ar conditions to remove the B-72 resin. Sintering temperatures varied between 500°C and 590°C for *p*-type fibers, and 500°C and 580°C for *n*-type fibers.

For the bulk materials used to fabricate the fibers, Seebeck coefficients and electrical conductivities were measured using a commercial unit (ZEM-3; ULVAC, Japan). For the fibers, electrical property characterization was conducted at room temperature. Seebeck coefficients were measured using an in-house apparatus (Fig. 1a) where voltage along the fiber direction was measured by a multimeter while the temperature difference was determined using thermocouples. Electrical resistivity was calculated from the resistance and the geometry of the fibers. Cross-sections of the fibers were examined using a scanning electron microscope (SEM).

Copper contacts were attached to glass substrates. Sintered TE fibers were cut and glued onto copper electrodes using silver paste. Power output and the *I*–*V* behavior of the TE modules were characterized using an in-house setup, illustrated in Fig. 1b. A variable resister (R_1) was used to simulate the external load. The output voltage, V_1, was measured using a multimeter; while the output current, I, was determined from the voltage (V_0) across a standard resister (R_0) such that $I = V_0/R_0$. Thin film thermocouples were placed next to the copper contacts to measure the hot-side and cold-side temperatures.

RESULTS AND DISCUSSION

In this proof-of-concept study, fixed ratios between the B-72 resin and the MEK solvent (1:1 weight ratio) and between B-72 and the TE phase (1:1 volumetric ratio) were used. This combination was used because the resultant powder/B-72/MEK paste could be easily extruded through a manually operated syringe and the resultant fibers could be formed in a continuous manner. As will be discussed

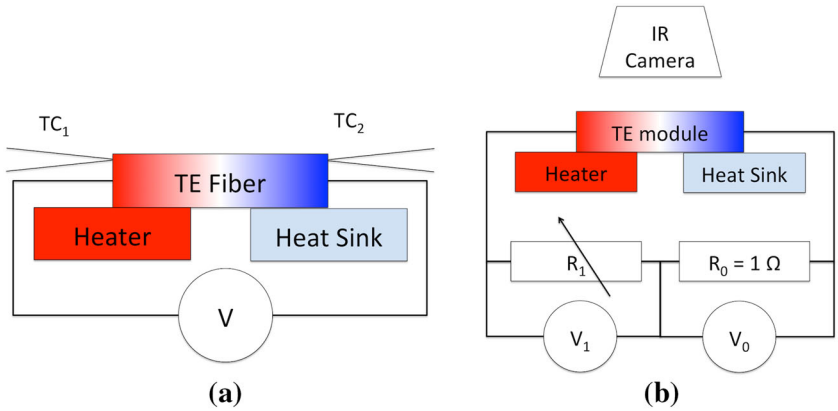

Fig. 1. Schematics showing the configurations used to determine (a) the Seebeck coefficient and (b) the power output.

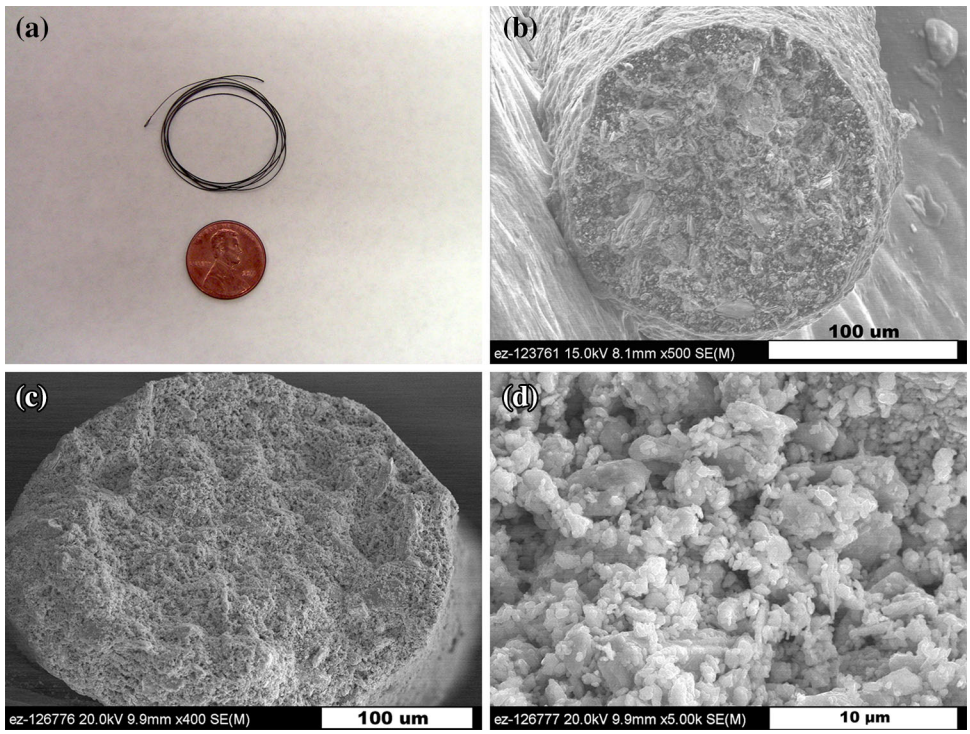

Fig. 2. (a) An as-extruded fiber, (b) its cross-section, and (c, d) a *p*-type fiber sintered at 590°C in vacuum for 4 h.

later, higher concentrations of the TE phase may be desired to achieve higher sintered density, which may be realized by the assistance of a mechanical pumping system that could provide higher pressure during extrusion. A systematic examination on the effect of relative amount of TE powders, the polymer resin, and the solvent will be the focus of follow-up studies.

Figure 2a shows a picture of a typical as-extruded fiber. In their unsintered "green" state, these fibers were very flexible and could be bent into various shapes with different radii. While the fibers could be fabricated in a continuous manner, their diameter was determined by the aperture size of the syringe nozzles. In this study, fibers with diameters of 100 μm and 200 μm were fabricated (Fig. 2b) and it is expected that this method may be used to manufacture fibers with diameters ranging between tens of microns to millimeters. Furthermore, since the length of the fibers could be extended in a continuous manner, TE elements with large length-to-area ratios could be easily obtained. For example, typical length-to-area ratios of the fibers fabricated in this study were of the order of 1×10^5 mm^{-1}.

After extrusion, removal of the polymeric phase was achieved by sintering either in vacuum tubes or in a flowing argon atmosphere. However, sintering in the flowing argon led to significant material loss

Table I. Comparison of thermoelectric properties between fiber and bulk materials

	S (μV/K)	ρ (mΩ-cm)	PF (μW/cm-K^2)
p-type ($Bi_{0.5}Sb_{1.5}Te_3$)			
Bulk	223	1.4	35
Fibers	179 to 193	14.1 to 18.8	1.7 to 2.6
n-type ($Bi_2Te_{2.7}Se_{0.3}$)			
Bulk	−250	2.93	21.5
Fibers	−207 to −268	153 to 189	0.3 to 0.4

S Seebeck coefficient, ρ electrical resistivity, *PF* power factor = S^2/ρ.

and thus was discontinued. After sintering at the maximum sintering temperatures, i.e. 590°C for *p*-type materials and 580°C for *n*-type materials, the relative densities of the fibers were approximately 75–80% of the bulk materials as determined from the sample mass and the geometry. Residual porosities in the sintered fibers can be clearly seen from the SEM images (Fig. 2c and d). The cross-sectional view of a *p*-type fiber vacuum-sintered at 590°C for 4 h is shown in Fig. 2c. Uniform distribution of micro pores can be observed. A higher magnification SEM image (Fig. 2d) further illustrates the micron-sized pores distributed between the TE grains. Sintering at higher temperatures was attempted to increase the density, which, however, led to significant material loss due to the low melting points of these materials (607°C for the *p*-type composition and 600°C for the *n*-type composition). On the other hand, extended holding time (>4 h) at the maximum sintering temperatures did not further increase the density.

Electrical resistivity of the sintered fibers was strongly affected by the sintering temperature such that increasing the sintering temperature led to decreased resistivity. In contrast, sintering time had a minor effect on the electrical resistivity. Electrical resistivity of the sintered fibers was as low as 14.1 mΩ-cm for *p*-type fibers sintered at 590°C and 153 mΩ-cm for *n*-type fibers sintered at 580°C, which, however, were much higher than the corresponding bulk materials (Table I).

Various factors could contribute to the reduced electrical conductivity including porosity, sintering-induced compositional change, and grain boundary effect. Large residual porosity in the sintered fibers was observed (Fig. 2c and d). Various empirical and analytical relationships have been developed to describe the effect of porosity, *P*, on the electrical conductivity of the powder compacts.[14,15] At low porosities, e.g., $P < 0.3$, Montes et al. showed that the following equation could well fit the data of iron, nickel, aluminum, and titanium powder compact[14]:

$$\sigma = \sigma_0(1 - P/P_C)^2 \tag{1a}$$

where σ and σ_0 are the electrical conductivities of the porous and fully dense materials, and P_C is the porosity related to the maximum packing density of the powder prior to compaction, which is affected by the size distribution and shape of the powders. The value of P_C varied between 0.52 for aluminum and 0.90 for nickel.[14] For powders with higher porosities ($0.3 < P < 0.75$), Zhu et al. found the $\sigma - P$ relationship of titanium and Ti-6Al-4V could be better described by[15]:

$$\sigma = \sigma_0\left(\frac{1 - P/P_C}{1 + kP}\right) \tag{1b}$$

where k is a constant related to the pore characteristics.

Assuming materials used in the current study follow Eq. 1a and the P_C value was roughly 0.7, the relative electrical conductivity, σ/σ_0, would be in the range of 25–35% for porosities between 0.2 and 0.25 (relative density 75–80%). In contrast, as shown in Table I, the relative conductivities with respect to the bulk materials were 7.5–10% for *p*-type and 1.5–2% for *n*-type fibers, which were much lower than the values estimated using Eq. 1a. Therefore, residual porosity may only have a minor effect on the reduced electrical conductivity. On the other hand, it is worth noting that Pachero et al.[17] observed that porosity had a smaller effect on electrical conductivity of *p*-type Bi_2Te_3-based materials than the *n*-type. For spark plasma-sintered *p*-type $Bi_{0.52}Sb_{1.48}Te_3$, the electrical conductivity reduced from 101 S/cm to 57 S/cm (43% reduction) when the relative density dropped from 98.2% to 92.6%. In contrast, electrical conductivity of *n*-type $Bi_2Te_{2.73}Se_{0.27}$ decreased from 986 S/cm to 138 S/cm (86% reduction) when the relative density changed from 97.5% to 91.5%. However, the authors did not offer an explanation for why *p*-type and *n*-type showed different dependence of electrical conductivity on density.[17]

Our measurement on bulk materials indicated that the electrical conductivity was very sensitive to the composition. For example, when the *n*-type composition was changed from $Bi_2Te_{2.7}Se_{0.3}$ to $Bi_2Te_{2.713}Se_{0.304}$, the electrical resistivity was reduced from 2.93 mΩ-cm to 1.22 mΩ-cm likely because Te and Se act as electron donors. To determine the composition of the sintered fibers, energy dispersive

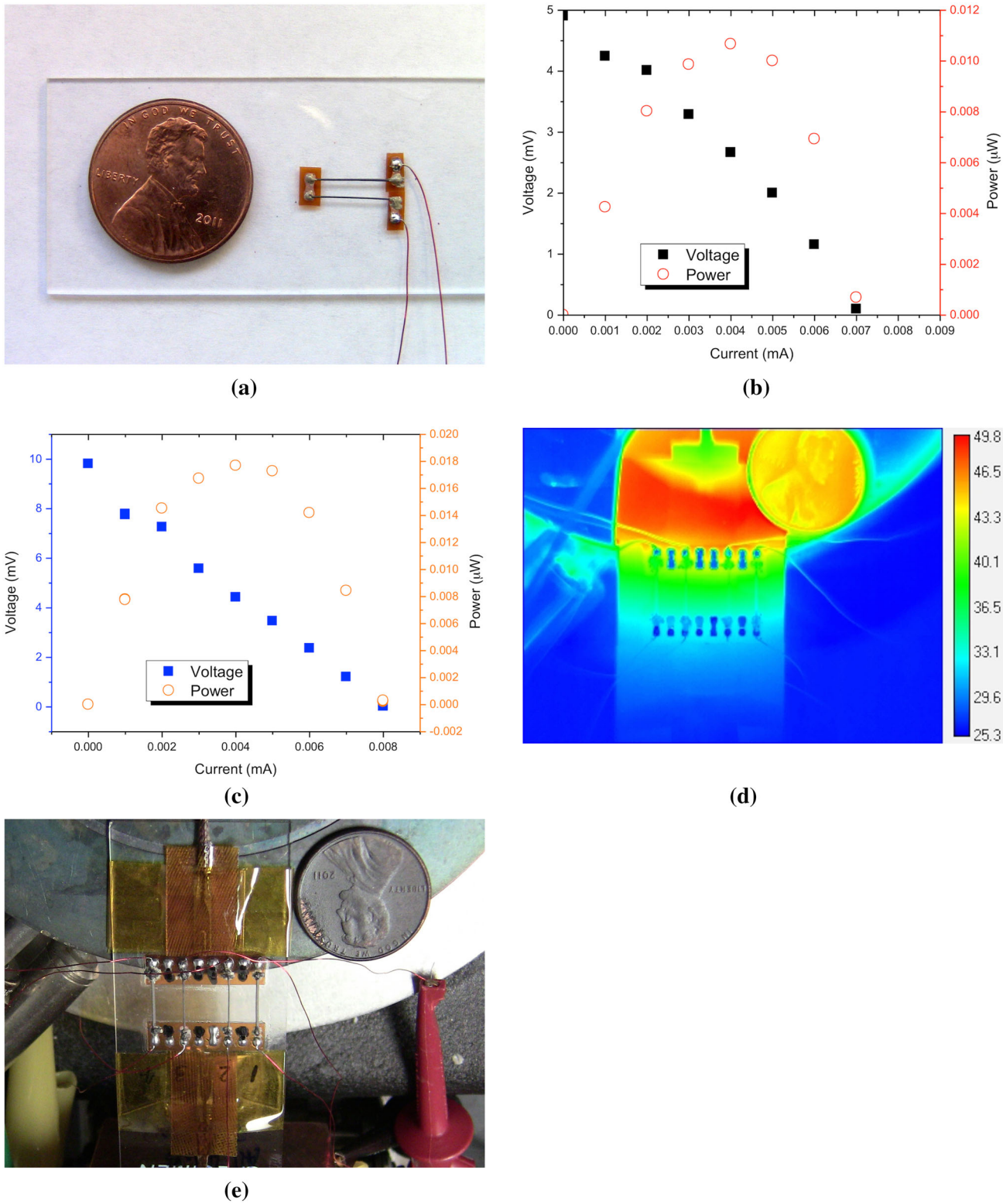

Fig. 3. (a) Prototype miniature uni-couple fabricated from sintered fibers and (b) its performance under a 12°C temperature difference. (c) *I–V* curve and power output of a module consisting of two uni-couples connected in series. (d) Infrared image of a prototype module consisting of two unicouples showing the temperature distribution in the module at equilibrium, and (e) its corresponding digital picture.

x-ray spectroscopy (EDS) was used to perform the chemical analysis. Compositional differences were observed between the fibers and the bulk materials, especially for the *n*-type fibers. Compared to the nominal composition of $Bi_2Te_{2.7}Se_{0.3}$, the composition of *n*-type fibers changed to $Bi_2Te_{2.894}Se_{0.368}$

after 4 h of sintering at 580°C. It was unexpected that the sintered *n*-type fibers were relatively poor in Bi since Te and Se are more volatile than Bi.[16] With a higher concentration of Te and Se, the electrical conductivity of the *n*-type fibers should be higher than the bulk, which contradicts the experimental observation in this study (Table I). Thus, the compositional shift may not be responsible for the reduced conductivity of the sintered fibers.

The low electrical conductivity may also be due to grain boundary contamination. For Bi_2Te_3-based materials, oxides such as Bi_2O_3 may form at grain boundaries and result in a reduction of electrical conductivity by as much as one order of magnitude.[17] However, in this study, it is difficult to determine whether there was significant amount of oxide using the EDS technique because sample surfaces could be easily contaminated by air during EDS sample preparation and mounting. On the other hand, as demonstrated in various ceramic systems, grain boundary resistivity may be indirectly measured by the AC impedance spectroscopy method,[18,19] which will be explored in future work.

The Seebeck coefficient of the fibers, on the other hand, exhibited comparable values to the bulk materials (Table I), implying that the Seebeck coefficient was not significantly affected by the sintering. However, due to the high resistivities, it is not surprising that the power factor of the sintered fibers was lower than the corresponding bulk materials (Table I). Although no thermal conductivity measurement was performed in the current study, it is expected that sintered fibers would possess lower thermal conductivities than the bulk materials, since the relationship shown in Eq. 1a could also be utilized to describe the effect of porosity on the thermal conductivity of sintered powder compacts.[14]

Figure 3a is a picture of a prototype miniature uni-couple fabricated from the sintered fibers and Fig. 3b shows its power output performance when the temperature gradient was approximately 12°C. The *I–V* curve of the uni-couple was nearly linear with an open-circuit voltage of 5 mV and a short-circuit current of 7 μA. The maximum output power was 10 nW when the output voltage was 2.6 mV.

Higher output power could be achieved by connecting multiple uni-couples either in series (with higher output voltage) or in parallel (with higher output current). For example, Fig. 3c shows the performance of two uni-couples connected in series, where the maximum output power was increased to 18 nW and the corresponding output voltage was increased to 4.8 mV. Figure 3d is the infrared image of this two uni-couple module showing the temperature distribution at thermal equilibrium; the hot size and cold side temperatures were approximately 42°C and 30°C, respectively. The corresponding picture of this module is shown in Fig. 3e. Prototype modules consisting of up to 4 uni-couples (8 fiber elements) were constructed and the power output and the voltage (or the current) were quadrupled compared to single uni-couples.

Due to the large electrical resistivity (Table I), these prototype uni-couples and modules fabricated from such fibers showed poor performance in terms of power output. Therefore, further studies are highly desirable to seek improved sintering conditions to optimize the fiber compositions and to reduce their porosity. As previously discussed, further increase in the sintering temperature would lead to significant material loss and fiber disintegration. Therefore, a potential processing parameter to explore is the initial volume fraction of the TE phase, which is currently fixed at 50 vol.% but could be increased in future studies. In addition, one could change the composition of the starting bulk materials to account for the elemental loss during sintering.

SUMMARY

A method based on powder processing and extrusion was developed to fabricate TE fibers with sub-millimeter diameters and large length-to-area ratios. The as-extruded fibers were very flexible and could be formed into various shapes. Vacuum sintering was used to remove the non-TE polymeric phase. The sintered fibers possessed Seebeck coefficients similar to the bulk materials but very high electrical resistivity, which may be related to residual porosity and grain boundary contamination. Consequently, the power outputs of the prototype uni-couples and modules were very low while the output voltages could reach the millivolt range. Further improvement in reducing the electrical resistivity is a key factor to develop high-performance TE fibers using this method. Future studies will include analysis of the grain boundary effect on the electrical resistivity and improvement in processing parameters to reduce porosity, compositional shift, and contamination.

ACKNOWLEDGEMENT

The research was sponsored by the ORNL Laboratory Directed Research and Development Seed Money Program, under DOE contract DE-AC05-00OR22725 with UT-Battelle, LLC.

REFERENCES

1. L.E. Bell, *Science* 32, 1457 (2008).
2. J.L. Bierschenk, *Energy Harvesting Technologies*, ed. S. Priya and D. Inman (New York: Springer, 2009), p. 337.
3. H.J. Goldsmid, *Introduction to Thermoelectricity* (New York: Springer, 2010), p. 167.
4. K. Uemura, CRC Handbook of Thermoelectrics, ed. D.M. Rome (CRC., New York, 1995).
5. I. Boniche, S. Masilamani, R.J. Durscher, B.C. Morgan, and D.P. Arnold, *J. Electro. Mater.* 38, 1293 (2009).
6. D.E. Wesolowski, R.S. Goeke, A.M. Morales, S.H. Goods, P.A. Sharma, M.P. Saavedra, K.R. Reyes-Gil, W.C.G. Neel, N.Y.C. Yang, and C.A. Apblett, *J. Mater. Res.* 27, 1149 (2012).
7. Q. Zhang, Y. Sun, W. Xu, and D. Zhu, *Adv. Mater.* (2014). doi:10.1002/adma.201305371.

8. Y. Chen, Y. Zhao, and Z. Liang, *Energy Environ. Sci.* 8, 401 (2015).
9. D. Madan, A. Chen, P.K. Wright, and J.W. Evans, *J. Appl. Phys.* 109, 034904 (2011).
10. M.-K. Kim, M.-S. Kim, S. Lee, C. Kim, and Y.-J. Kim, *Smart Mater. Struct.* 23, 105002 (2014).
11. I. Shiota, H. Kohri, M. Kato, I.J. Ohsugi, *Proc. 2006 ICT*, 247 (2006).
12. S. Baskaran, S.D. Nunn, D. Popovic, and J.W. Halloran, *J. Am. Ceram. Soc.* 76, 2209 (1993).
13. F. Ren, H. Wang, P. Menchhofer, and J. Kiggans, *Appl. Phys. Lett.* 103, 221907 (2013).
14. J.M. Montes, J.A. Rodríguez, and E.J. Herrera, *Powder Metall.* 46, 251 (2003).
15. K. Zhu, C.-F. Li, and Z.-G. Zhu, *Chin. Phys. Lett.* 24, 187 (2007).
16. D.R. Lide, *CRC Handbook of Chemistry and Physics*, 96th ed. (Swindon: Taylor & Francis, 2015–2016), section 6.
17. V. Pachero, H. Gorlitz, N. Peranio, Z. Aabdin, O. Eibl, *Thermoelectric Bi2Te3 Nanomaterials*, ed. O. Eibl, K. Nielsch, N. Peranio, F. Volklein (Weinheim: Wiley-VCH, 2015), p. 99.
18. X. Guo and R. Waser, *Prog. Mater Sci.* 51, 151 (2006).
19. M. Gerstl, E. Navickas, G. Friedbacher, F. Kubel, M. Ahrens, and J. Fleig, *Solid State Ion.* 185, 32 (2011).